SOLVATION AND ION PAIR ASSOCIATION IN AQUEOUS METAL SULFATES: INTERPRETATION OF NDIS RAW DATA BY ISOBARIC–ISOTHERMAL MOLECULAR DYNAMICS SIMULATION

Ariel A. CHIALVO[a,*] and J. Michael SIMONSON[b]

[a] *Chemical Sciences Division, Geochemistry and Interfacial Science Group, Oak Ridge National Laboratory, Oak Ridge, TN 37831-6110, USA; e-mail: chialvoaa@ornl.gov*

[b] *Center for Nanophase Materials Sciences, Oak Ridge National Laboratory, Oak Ridge, TN 37831-6496, USA; e-mail: simonsonjm@ornl.gov*

Received October 29, 2009
Accepted January 12, 2010
Published online April 15, 2010

Dedicated to Professor Ivo Nezbeda on the occasion of his 65th birthday.

We analyzed the solvation behavior of aqueous lithium, nickel, and ytterbium sulfates at ambient conditions in terms of the relevant radial distributions functions and the corresponding first-order difference of the sulfur-site neutron-weighted distribution functions generated by isothermal-isobaric molecular dynamics simulation. We determined the partial contributions to the neutron-weighted distribution functions, to identify the main contributing peaks of the corresponding radial distribution functions, and the effect of the contact ion-pair configuration on the resulting water's hydrogen coordination around the sulfate's sulfur site. Finally, we assessed the extent of the ion-pair formation according to Poirier–DeLap formalism and highlighted the significant increase of the ion-pair association exhibited by these salts with cation charge.

Keywords: Neutron diffraction; Molecular dynamics; Ion pairs; Anion hydration; NDIS; Coordination number; Radial distribution functions.

Ion-pair recognition and separation by synthetic hosts is an effective approach for the recovery of salts from dilute aqueous solutions, i.e., the simultaneous extraction of the cation species as well as the anions. Early efforts on solvent ion extraction placed more emphasis on the design of ion receptors for cation complexation, while anion co-extraction selectivity followed from their solvation behavior[1,2]. Because the success of an extraction process has been measured in terms of separation selectivity, the driving force behind new developments to increase selectivity has aimed at ways to

Collect. Czech. Chem. Commun. 2010, Vol. 75, No. 4, pp. 405–424

doi:10.1135/cccc2009535

tailor the system at a molecular level to maximize it by manipulation of the receptors and the solvating environment.

Typically, separation selectivity is governed by microscopic phenomena that promote either bias or recognition[3]. Consequently, the general expectation on the extent of the salt extraction was roughly dictated by the Hofmeister selectivity[4]. However, when introducing ion-receptors into the extractant phase as facilitators of salt extraction, there is no reason to expect a Hofmeister trend especially when considering that ions–macromolecule interactions might be more favorable for anions than cations.

A recurrent concept underlying the extractive salt separation is the so-called Hofmeister behavior (or lack of, i.e., Hofmeister bias), when referring to the relative effectiveness of anions and cations to affect the outcome[5]. In particular, anti-Hofmeister behavior has been observed in a large number of the anion separations, and it is obviously of great interest to unravel the actual molecular mechanism in a rational search for ways to overcome it[6–8]. Obviously, species solvation plays a pivotal role in determining the sought mechanism, and consequently, on the anion–cation pair formation.

The solvation of multi-charged anions plays an important role in biological systems and separation processes involving the Hofmeister series[5]. Sulfates can be described as prototypical multi-charged anions whose tetrahedral distribution of oxygen sites facilitates the understanding of the impact of the anion–water interactions on the resulting solvation behavior. The presence of ions in an otherwise pure aqueous environment modifies the microstructure of the solvent, and consequently, the thermophysical properties of the resulting aqueous solution. This structural water perturbation around the ions is the consequence of the ion–water (and eventually ion–ion) interactions not present in the pure solvent, i.e., the difference of strength between the solvent–solvent and the ion–solvent interactions macroscopically manifested as solution nonideality[9,10].

An early view of the structure of aqueous electrolyte solutions introduced the concept of structure-maker and structure-breaker ions, introduced as a measure of the order/disorder induced on the surrounding solvent relative to that of the pure solvent. This picture also provides the idea of the ion solvation (hydration) numbers as the estimated number of solvent (water) molecules coordinated with the ion under consideration, a concept that has allowed a simplified interpretation and modeling of these systems[11]. Even though there are rather complete compilations of solvation (hydration) numbers[12,13], they are based on indirect experimental determinations (e.g., mobility, compressibility, and dielectric measurements) resulting in a wide-

spread and inconsistent set of results[14] whose usefulness might be questioned[15].

From a basic microstructural viewpoint, solvation numbers are directly linked to the number of coordinated solvent molecules around the species under consideration, consequently, the best approach to their assessment is through the determination of the corresponding ion–solvent radial distribution function. Among others, neutron diffraction with isotope substitution (NDIS) is a versatile tool for the determination of the microstructure of aqueous electrolytes, e.g., the ion–water correlations by the first-order difference method[16]. The suitability of this method depends on the ions having different isotopic coherent scattering lengths while the successful implementation and the outcome of the experiments depends strongly on the interpretation of the shape, location, and resolution of scattering peaks, and in particular, on de-convoluting the peak overlapping associated with ion-pairing[17,18].

From a strictly microstructural viewpoint, the formation of a contact ion pair in aqueous solutions of a salt $M^{\nu+}X_n^{\nu-}$ is a penetration of solvation shell of $M^{\nu+}$ into that of $X^{\nu-}$. In terms of NDIS data, this formation leads to an overlapping of the $M^{\nu+}$–$X^{\nu-}$ with either the H–$M^{\nu+}$ (H–$X^{\nu-}$) or O–$M^{\nu+}$ (O–$X^{\nu-}$) contributions to the corresponding total structural factors, and represented as a distortion of the normal shape of either the first or the second peak of the first-order difference of the neutron-weighted distribution functions in heavy water[19,20].

In this context, as discussed in details elsewhere[19–21], molecular-based simulation can help in the interpretation of the diffraction data, because it provides the unambiguous link between the system structure under study and the corresponding neutron-weighted distribution functions, consequently, simulation offers a route for the unambiguous test of consistency and/or accuracy for the methods and hypothesis used in the extraction of structural information from diffraction experiments.

In what follows, we introduce the foundation for our analysis in section Fundamentals, and the intermolecular model as well as the simulation methodology in section Potential Models and Simulation Methodology. In section Microstructural Results, we present and discuss the simulation results and final remarks are given in Conclusions.

FUNDAMENTALS

The systems of interest here comprise aqueous solutions of metal sulfates, $M_2^{z+}(SO_4^{2-})_{z+}$, where M^{z+} {Li^+, Ni^{2+}, Yb^{3+}}, and involve the following total structure factor $F(k)$ defined as[22],

$$F(k) = \sum_i \sum_j c_i c_j b_i b_j \left(S_{ij}(k) - 1\right) \qquad (1)$$

where $k = (4\pi/\lambda)\sin(\theta/2)$ is the magnitude of the scattering vector as a function of the wavelength λ of the incident neutrons and the scattering angle θ. In Eq. (*1*), c_i and b_i denote the atomic fraction and the coherent scattering length of atomic species i for neutrons, $S_{ij}(k)$ is the partial structure factor describing the correlation between atoms of types i and j, i.e.,

$$S_{ij}(k) = 1 + (4\pi\rho_o / k)\int_0^\infty \left(g_{ij}(r) - 1\right) r \sin(kr)\,\mathrm{d}r \qquad (2)$$

where ρ_o and $g_{ij}(r)$ are the atomic number density of the solution and the radial pair distribution function for *ij*-interactions. Note that the summations in Eq. (*1*) involve all four species, i.e., H, O, S, and M^{z+}, where the O contributions are from the water as well as the sulfate ions, consequently $F(k)$ comprises 12 *ij*-pair contributions.

Obviously, $F(k)$ can be generated either by simulation or experimentally by neutron scattering. What is measured in the latter is the neutron scattering differential cross section $F_o(k)$, i.e.,

$$F_o(k) = \frac{\mathrm{d}\sigma}{\mathrm{d}\Omega} = F(k) + \sum_i c_i \sigma_i^{\mathrm{total}} / 4\pi + \text{relevant corrections} . \qquad (3)$$

Therefore, the sought $F(k)$ becomes available after subtracting the total (coherent plus incoherent) $\sigma_i^{\mathrm{total}}$ cross section for nucleus i, and correcting for inelastic (Placzek corrections), multiple scattering, as well as for sample and container absorption[23]. Obviously, these corrections introduce uncertainties into the analysis of the experimental data, while molecular simulation directly provides all radial distribution functions and consequently $G(r)$, i.e., the real space counterpart of $F(k)$.

Because the real space is the natural simulation environment, from a simulation perspective it is advantageous to deal with the neutron-weighted real space distribution function $G(r)$, rather than $F(k)$, i.e.,

$$G(r) = \sum_i \sum_j c_i c_j b_i b_j \left(g_{ij}(r) - 1 \right) \tag{4}$$

as a linear combination of the radial pair distribution functions $g_{ij}(r)$, i.e.,

$$g_{ij}(r) = 1 + (1 / 2\pi^2 \rho_o r) \int_0^\infty \left(S_{ij}(k) - 1 \right) k \sin(kr)\, \mathrm{d}k \,. \tag{5}$$

In order to extract some useful microscopic information about the solvation behavior of the ions we need to decouple the most relevant contributions to Eq. (*4*) by canceling the largest contributions from the (light or heavy) water–water correlations, i.e., either from $g_{OH}(r)$ and $g_{HH}(r)$ or from $g_{OD}(r)$ and $g_{DD}(r)$. This is usually achieved by the first-order difference method[24] that comprises a set of two diffraction experiments, involving two identical solutions except for the different isotopic states of an atom in the polyatomic ion (sulfur in this case).

For an aqueous sulfate solution the sulfur-site first difference of total neutron-weighted distribution functions reads,

$$\begin{aligned} \Delta G_S^{\mathrm{solv}}(r) &= G_{^{33}S}^{\mathrm{solv}}(r) - G_{^{\mathrm{nat}}S}^{\mathrm{solv}}(r) = \\ &= A_S \left(g_{O_w S}(r) - 1 \right) + B_S \left(g_{DS}(r) - 1 \right) + C_S \left(g_{HS}(r) - 1 \right) + \\ &+ D_S \left(g_{MS}(r) - 1 \right) + E_S \left(g_{SS}(r) - 1 \right) + F_S \left(g_{SO_s}(r) - 1 \right) \end{aligned} \tag{6}$$

or its normalized form,

$$\begin{aligned} \Delta G_S^{\mathrm{solv,norm}}(r) = \big(& A_S g_{O_w S}(r) + B_S g_{DS}(r) + C_S g_{HS}(r) + \\ & + D_S g_{MS}(r) + E_S g_{SS}(r) + F_S g_{SO_s}(r) \big) / \sum_S^{\mathrm{solv}} . \end{aligned} \tag{7}$$

The superscript "solv" in Eqs (*6*) and (*7*) highlights the fact that the solvent is light, heavy, or a mixture of both water's isotopologues, $\sum_S^{\mathrm{solv}} = A_S + B_S + C_S + D_S + E_S + F_S$, where these coefficients are defined in the Appendix A. In particular, note that $B_S = -C_S$ for $c_D/c_H = -b_H/b_D \cong 0.561$, the so-called null water composition, so that after invoking the quasi-isomorphic condition $g_{SD}(r) \cong g_{SH}(r)$, Eq. (*7*) simplifies to

$$\Delta G_{\mathrm{S}}^{\mathrm{null,norm}}(r) = \frac{A_{\mathrm{S}}\, g_{\mathrm{O_wS}}(r) + D_{\mathrm{S}}\, g_{\mathrm{MS}}(r) + E_{\mathrm{S}}\, g_{\mathrm{SS}}(r) + F_{\mathrm{S}}\, g_{\mathrm{SO_s}}(r)}{A_{\mathrm{S}} + D_{\mathrm{S}} + E_{\mathrm{S}} + F_{\mathrm{S}}} \qquad (8)$$

where the contribution $F_{\mathrm{S}}\, g_{\mathrm{SO_s}}(r)/(A_{\mathrm{S}} + D_{\mathrm{S}} + E_{\mathrm{S}} + F_{\mathrm{S}})$ can be safely neglected because it is more than one order of magnitude smaller than any other in Eq. (*8*). As already discussed by the authors[20] the significance and practical implications of Eq. (*8*) hinge around the absence of any ion–deuterium and/or ion–hydrogen contributions to $\Delta G_{\mathrm{S}}^{\mathrm{null,norm}}(r)$ and therefore, of any potential S–H and/or S–D peak overlapping with that from the corresponding S–M pair representing an ion-pair contribution. While a full discussion of the experimental difficulties underlying this method is beyond the scope of this work, we should point out that being able to detect, and subsequently isolate, S–M pair formation is central to either the accurate determination of or the assessment of its effects on water–sulfate coordination[19,21].

In order to discuss the effect of ion-pairing on the $\Delta G_{\mathrm{S}}^{\mathrm{solv,norm}}(r)$'s peaks, we must also be able to assess the extent of such pairing according with an unambiguous formalism, i.e., in terms of a well-defined degree of ion-pair association α_{+-}. For that purpose we turn to a rigorous, yet little used, theoretical approach developed more than forty years ago by Poirier and DeLap[25], i.e.,

$$\alpha_{-+} = \int_0^{d_{-+}} G_{-+}(r)\,\mathrm{d}r \qquad (B1)$$

where d_{-+} defines the upper bound for the count of M^{z+}–SO_4^{2-} pairs, and $G_{-+}(r)\Delta r$ is the probability of finding the M^{z+} in the spherical shell of thickness Δr, separated by a distance r from the SO_4^{2-}, when neither M^{z+} nor SO_4^{2-} forms any additional pair within the distance r (see Appendix B for details in the case of $z = 2$).

POTENTIAL MODELS AND SIMULATION METHODOLOGY

In order to study the solvation behavior of the sulfates and to illustrate the issues discussed above, we performed isobaric–isothermal molecular dynamics simulations of aqueous metal sulfate solutions involving mono-, di- and trivalent cations at ambient conditions. For that purpose we have chosen simple but reliable intermolecular potential models including the rigid SPC/E water model[26], and Dang et al.[27], Wallen et al.[28], van Veggel et al.[29] and Cannon et al.[30] for the parameterization of the lithium, nickel, ytterbium and sulfate ions, respectively. All these potentials are represented in

terms of Lennard–Jones (LJ) and electrostatic interactions whose unlike LJ-pair interactions are described by the Lorentz–Berthelot combining rules (Table I).

The isobaric–isothermal molecular dynamics simulations of the aqueous solutions were carried out according to a Nosé–Poincare symplectic integration algorithm[31] involving a total of 1372 particles at T = 298 K and P = 1 atm for the salt concentrations indicated in Table II, spanning 3 ns after 200 ps of equilibration time from the initial configuration.

From the simulated radial distribution functions we determined the neutron-weighted distribution functions $\Delta G_S^{\mathrm{solv,norm}}(r)$ for heavy water according to the Eqs (*7*) and (*9*). Moreover, we calculate the ions' coordination numbers according to their definitions and compared them against those from the first-

TABLE I
Lennard–Jones potential parameters and partial charges for the ion–ion interactions with I_{SO} = 1.49 Å (ref.[30])

ii Interaction	ε_{ii}/k, K	σ_{ii}, Å	q_i, e	Ref.
Li^+–Li^+	83.04	1.508	1.0	27
Ni^{2+}–Ni^{2+}	50.34	2.050	2.0	28
Yb^{3+}–Yb^{3+}	20.14	2.950	3.0	29
O_S–O_S	125.9	3.150	–1.10	30
S–S	125.9	3.550	2.40	30

TABLE II
Compositions of the aqueous systems studied at ambient conditions

Salt	Molality	Density, g/cc[a]
Li_2SO_4	0.26	1.023 ± 0.002
	0.60	1.058 ± 0.002
	0.87	1.084 ± 0.002
$NiSO_4$	0.52	1.077 ± 0.003
	1.02	1.147 ± 0.003
	1.78	1.255 ± 0.003
$Yb_2(SO_4)_3$	0.46	1.288 ± 0.008

[a] Resulting density at ambient conditions.

order difference scheme counterparts (see section Microstructural Results). Finally, we assess the degree of ion-pair formation, α_{-+}, based on Poirier–DeLap formalism involving the simulated $g_{M^{z+}SO_4^{2-}}(r)$.

MICROSTRUCTURAL RESULTS

In what follows we analyze the predicted solvation behavior of the sulfate ion for the three different counterions at ambient conditions in terms of relevant radial distribution functions. In Fig. 1, we display a representative comparison of the microstructure of water around the sulfur site of the aqueous sulfate as a function of the counterion present. A notable feature in this figure is the lack of water structure beyond the two main peaks, i.e., beyond 8 Å for all three systems, and the appearance of a shoulder after the first peak of the oxygen–sulfur pair interaction for the lithium sulfate solution. According to the definition of water coordination around the sulfur site, i.e., $n_S^O(d) = 4\pi\rho_O\int_0^d g_{OS}(r)r^2\mathrm{d}r$ and $n_S^H(d) = 4\pi\rho_H\int_0^d g_{HS}(r)r^2\mathrm{d}r$, this site is surrounded by approximately 13 ($d \cong 4.5$ Å), 14.5 ($d \cong 4.6$ Å) and 14.3 ($d \cong 4.5$ Å) water oxygens, as well as 9.6 ($d \cong 3.33$ Å), 11.2 ($d \cong 3.42$ Å) and 9.8 ($d \cong 3.37$ Å) water hydrogens when the counterions are lithium, nickel and ytterbium, respectively.

In Fig. 2, we display the comparison between the radial distributions for the (water oxygen)–(sulfate oxygen) pair (O–O_s) interactions for the same systems as in Fig. 1. Once again, this picture suggests the loss of water structure beyond 8 Å from any sulfate's oxygen site, with well defined first peaks for O–O_s and H–O_s interactions which are located at distances similar to those found for water–water interactions. However, we note two important differences with the latter, namely, the stronger H–O_s and the presence of secondary multiple peaks. In terms of coordination numbers, $n_{O_s}^O(d) = 4\pi\rho_O\int_0^d g_{OO_s}(r)r^2\mathrm{d}r$, these structures represent an average of about 2.3 ($d \cong 2.96$ Å), 3.4 ($d \cong 3.23$ Å) and 3.3 ($d \cong 3.2$ Å) water oxygens around each sulfate oxygens when the counterions are lithium, nickel and ytterbium, respectively. Note that, due to sharing hydration water molecules between the tetrahedral location of the sulfate oxygens, the reported oxygen coordination of the sulfur site is larger than what it would result by multiplying the number of sulfate oxygens to their own water oxygen coordination, i.e., 4 × (2.3, 3.4, 3.3).

The other relevant microstructural information connected to the occurrence of ion-pair association is portrayed in Figs 3–5, where we present the metal–sulfate pair distribution functions $g_{M-SO_4}(r)$ in comparison with the corresponding ion-pair distribution functions $G_{-+}(r)$ and the resulting de-

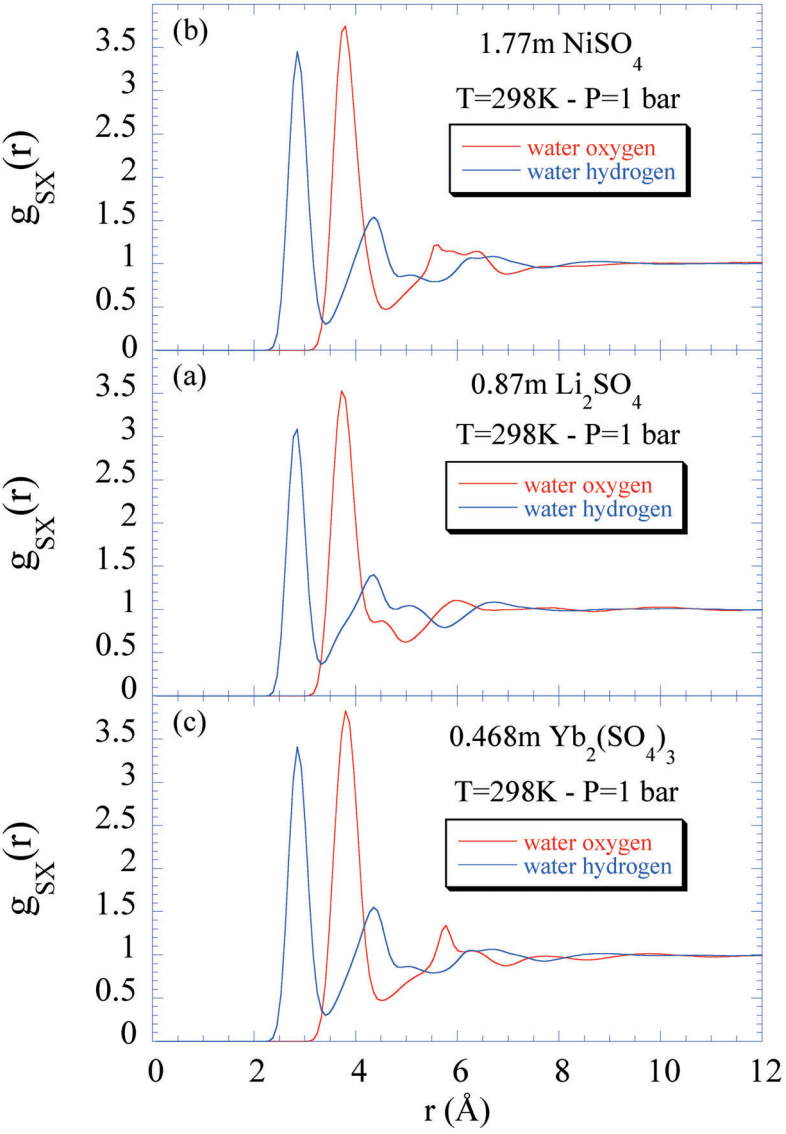

FIG. 1
Predicted radial distribution functions for the O–S and H–S interactions at ambient conditions: 0.87 m Li_2SO_4 (a), 1.77 m $NiSO_4$ (b), and 0.468 m $Yb_2(SO_4)_3$ (c)

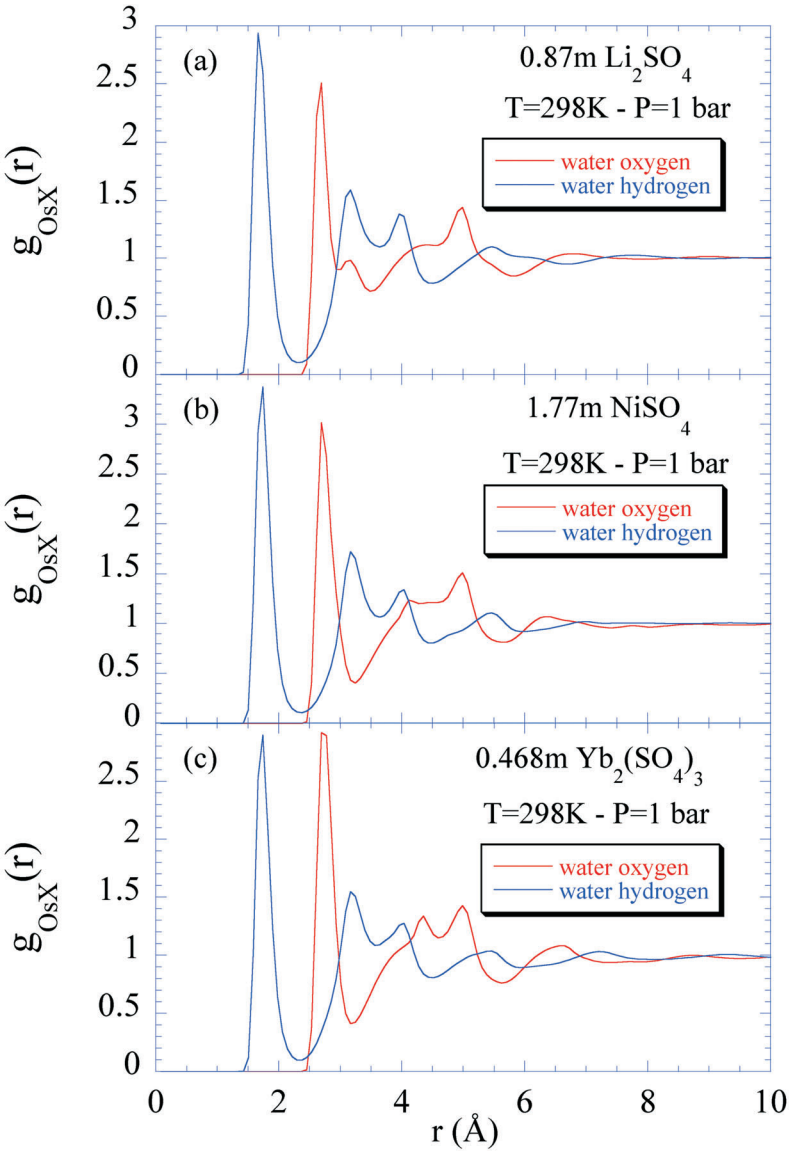

FIG. 2
Predicted radial distribution functions for the O–O_{SO_4} and H–O_{SO_4} interactions at ambient conditions: 0.87 m Li_2SO_4 (a), 1.77 m $NiSO_4$ (b), and 0.468 m $Yb_2(SO_4)_3$ (c)

gree of ion-pair association α_{-+} (discussed in section Potential Models and Simulation Methodology). The outstanding feature in these pictures is the relatively strong first peaks for the $g_{M-SO_4}(r)$ representing contact ion-pair conformations followed by weaker water-shared ion-pair configurations, exhibiting a deformed shape as either double peak (lithium) or as a right shoulder (nickel and ytterbium). The corresponding $G_{-+}(r)$ functions exhibit behavior similar to the corresponding $g_{M-SO_4}(r)$, though the magnitude of their peaks is much smaller (i.e., they are normalized to one), and predict

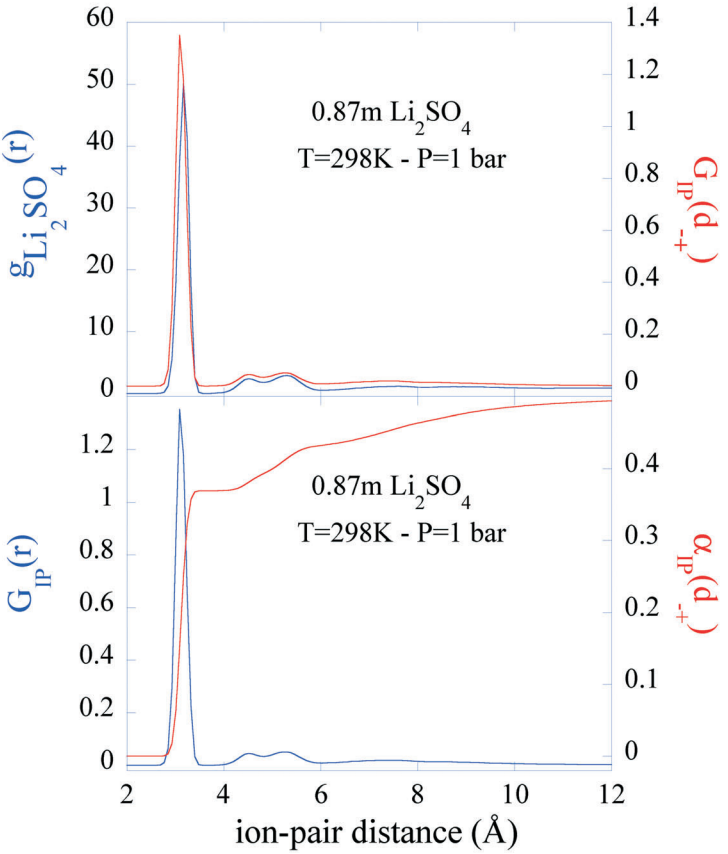

FIG. 3
Predicted radial distribution function for the M–SO_4 interactions, the ion-pair distribution, and its corresponding running degree of association for the 0.87 m aqueous Li_2SO_4 solution at ambient conditions

significant metal–sulfate pair association. The degrees of association for lithium sulfate are α(CIP) ≅ 0.37 and α(CIP + SShIP) ≅ 0.43, for nickel sulfate are α(CIP) ≅ 0.36 and α(CIP + SShIP) ≅ 0.72, while for ytterbium sulfate are α(CIP) ≅ 0.47 and α(CIP + SShIP) ≅ 0.59. These results suggest a clear trend for the extent of the ion-pair association α(CIP + SShIP), i.e., it increases with the ionic strength as we might have expected. However, note that the increase of ionic strength in these systems is dominated by the counterion charge, i.e., these results suggest that the degree of metal–sulfate pairing would follow the order $Li^+ < Ni^{2+} < Yb^{3+}$.

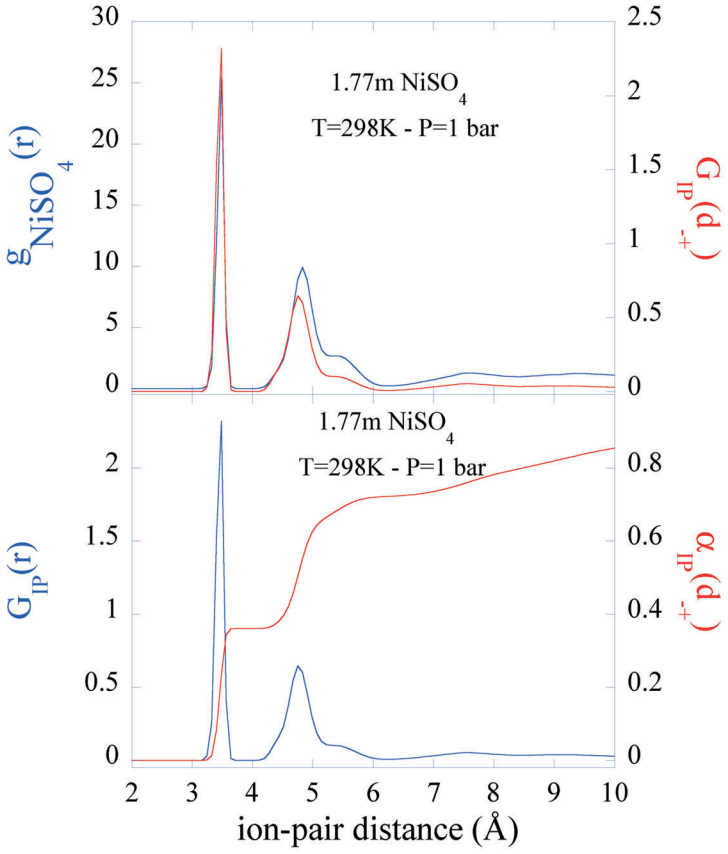

FIG. 4
Predicted radial distribution function for the M–SO_4 interactions, the ion-pair distribution, and its corresponding running degree of association for the 1.77 m aqueous $NiSO_4$ solution at ambient conditions

In Figs 6–8, we display the predicted normalized neutron-weighted distribution functions $\Delta G_S^{solv,norm}(r)$ in heavy water for the same three aqueous metal sulfates. In this representation we also show the four most relevant partial contributions to aid the interpretation of their participation in the resulting profile. For example, these pictures clearly indicate that the first peak of $\Delta G_S^{hw,norm}(r)$ is almost entirely defined by the H–S pair interactions, except for a small distortion at the valley of the peak resulting from the partial overlap of this with the first peak of the O_w–S and the M–S pair in-

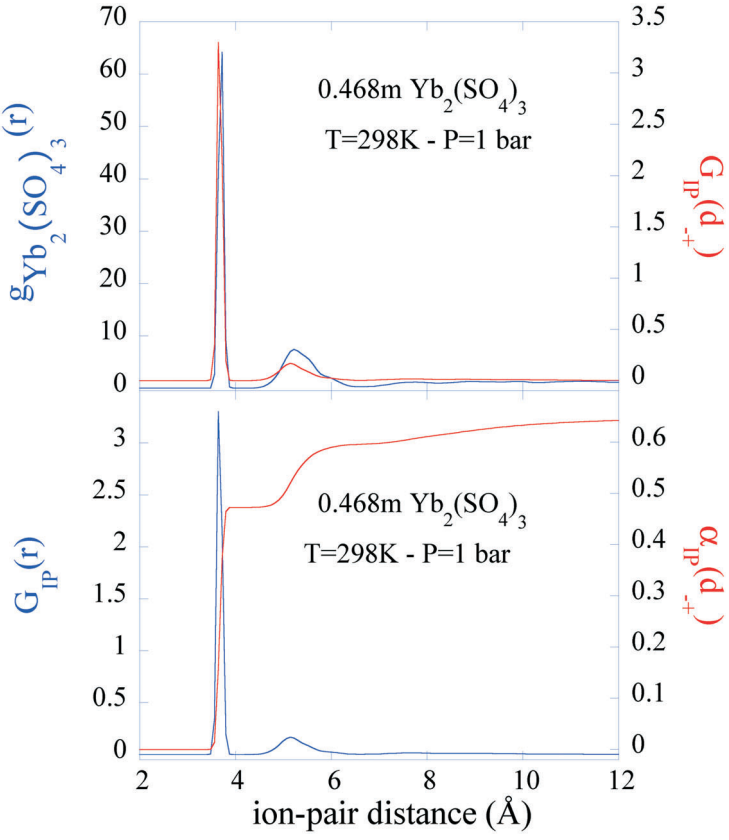

FIG. 5
Predicted radial distribution function for the M–SO_4 interactions, the ion-pair distribution, and its corresponding running degree of association for the 0.468 m aqueous $Yb_2(SO_4)_3$ solution at ambient conditions

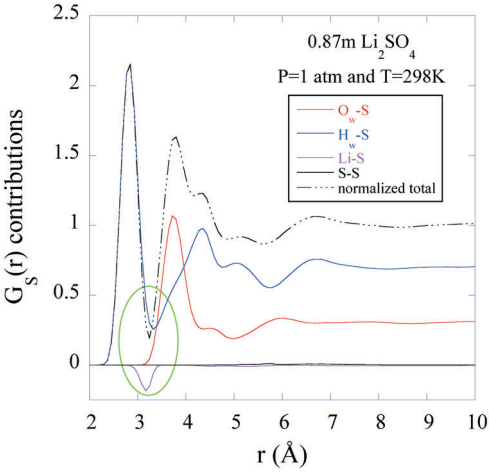

FIG. 6
Predicted sulfur-site neutron-weighted radial distribution function for the 0.87 m aqueous Li_2SO_4 solution at ambient conditions. Green circle highlights details of the peaks overlapping at the first valley

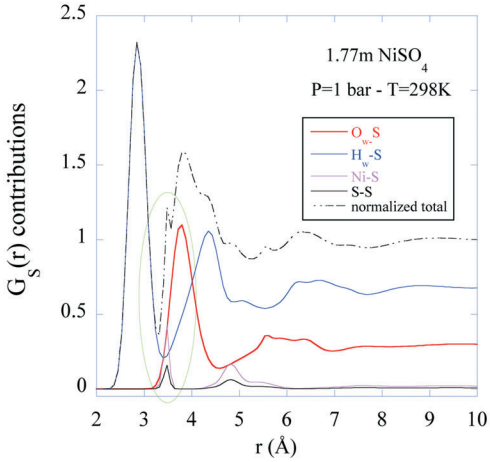

FIG. 7
Predicted sulfur-site neutron-weighted radial distribution function for the 1.77 m aqueous $NiSO_4$ solution at ambient conditions. Green circle highlights details of the peaks overlapping at the first valley

teractions. Note that the contact ion-pair peak contribution is negative for lithium, but positive for nickel and ytterbium whose main effects are highlighted by the green circles in Figs 6–8 as a shift to the left for the location of the valley (d* < d) and an effective reduction in the estimated water-hydrogen (H–S) coordination number, i.e.,

$$n_S^H(d^*) = 4\pi\rho_H \left(\sum\nolimits_S^{hw} / B_S \right) \int_0^{d^*} \Delta G_S^{hw,norm}(r) r^2 \, dr \, . \qquad (9)$$

TABLE III
Comparison of coordination numbers determined by the two approaches

Salt	Molality	Direct	$\Delta G_S(r)$ – based
Li_2SO_4	0.87	9.6	8.8
$NiSO_4$	1.78	11.2	10.9
$Yb_2(SO_4)_3$	0.46	9.8	9.8

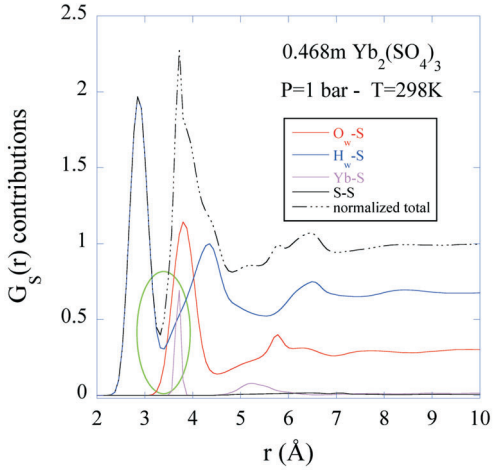

FIG. 8
Predicted sulfur-site neutron-weighted radial distribution function for the 0.468 m aqueous $Yb_2(SO_4)_3$ solution at ambient conditions. Green circle highlights details of the peaks overlapping at the first valley

The resulting coordination numbers around the sulfur site according to this expression are compared with those from the direct determinations in Table III. Note that the second peak of $\Delta G_S^{hw,norm}(r)$ is actually a combination of at least three contributions; namely, the first O_w–S peak, the second H–S peak, and the contact ion-pair configuration. Moreover, the second peak of $\Delta G_S^{hw,norm}(r)$ can exhibit a left shoulder that evolves into a small secondary peak with an increase of the salt concentration, as clearly depicted in Fig. 7 for the nickel sulfate.

CONCLUSIONS

We have analyzed the solvation behavior of aqueous sulfates involving lithium, nickel and ytterbium ions at ambient conditions in terms of the relevant radial distributions functions, and the corresponding first-order difference of the sulfur-site neutron-weighted distribution functions. We have taken advantage of the unmatched opportunity offered by molecular simulation to interpret the partial contribution to the neutron-weighted distribution functions, to identify the main peaks, and the effect of the contact ion-pair configuration on the resulting H–S coordination. Finally, we have determined the extent of the ion-pair formation, as contact and water-shared configurations, according to Poirier–DeLap formalism and concluded that these salts exhibit a rather significant association at composition close to saturation, i.e., at lower molality as cation charge increases from mono- to trivalent. We must recognize that while the extent of the ion pairing might be sensitive to the choice of force-field parameterization, the validity of the proposed interpretative analysis does not depend on that choice. However, if we intended to assess the accuracy of the simulation predictions for the ion pair association, then we would need the microstructural information from NDIS experiments whose interpretation will be facilitated by our proposed methods as discussed in details in refs[6–8].

APPENDIXES

Appendix A

Coefficients of the neutron-weighted distribution functions $\Delta G_S^{solv}(r)$

$$A_S = 2c_S c_{O_w} b_O ({}^{33}b_S - {}^{nat}b_S)$$

$$B_S = 2c_S c_D b_D ({}^{33}b_S - {}^{nat}b_S)$$

$$C_S = 2c_S c_H b_H ({}^{33}b_S - {}^{nat}b_S)$$

$$D_S = 2c_S c_M b_M ({}^{33}b_S - {}^{nat}b_S)$$

$$E_S = c_S^2 ({}^{33}b_S^2 - {}^{nat}b_S^2)$$

$$F_S = 2c_S c_{O_s} b_O ({}^{33}b_S - {}^{nat}b_S)$$

where the coherent scattering lengths have been taken from Sears' tabulation[32], i.e.,

$$b_O = 5.80 \text{ fm}$$

$$b_D = 6.671 \text{ fm}$$

$$b_H = -3.74 \text{ fm}$$

$${}^{33}b_S = 4.74 \text{ fm}$$

$${}^{nat}b_S = 2.847 \text{ fm}$$

$$b_{Li} = -2.22 \text{ fm}$$

$$b_{Ni} = 10.30 \text{ fm}$$

$$b_{Mg} = 5.375 \text{ fm}$$

$$b_{Yb} = 12.43 \text{ fm}$$

Appendix B

Definition of degree of M^{2+}–SO_4^{2-} pair association and its relation to the radial distribution function $g_{M^{z+}-SO_4^{2-}}(r)$ in the thermodynamic limit.

For the cases considered here the degree of M^{2+}–SO_4^{2-} pair association, α_{-+}, is defined as,

$$\alpha_{-+} = \int_0^{d_{-+}} G_{-+}(r)\,\mathrm{d}r \qquad (B1)$$

where d_{-+} denotes the largest distance where the M^{2+}–SO_4^{2-} pairs are counted, typically the location of the first (for contact ion pairs) or second

valley (for contact plus solvent-shared ion pairs) of $g_{M^{z+}-SO_4^{2-}}(r)$, and $G_{-+}(r)\Delta r$ is the probability of finding the SO_4^{2-} group in the spherical shell of thickness Δr, separated by a distance r from the M^{2+} ion, when neither the SO_4^{2-} nor the M^{2+} forms any additional pair within r. From a statistical mechanical point of view, $G_{-+}(r)$ can be written as the following integral equation,

$$G_{-+}(r) = 4\pi\rho_+ g_{-+}(r) r^2 P_-(r) P_+(r) \qquad (B2)$$

where $P_-(r)$ ($P_+(r)$) denotes the probability that an SO_4^{2-} (M^{2+}) separated by a distance r from an M^{2+} (SO_4^{2-}) does not form an ion pair with any other ion of the opposite charge, i.e.,

$$P_-(r) = 1 - \int_0^r G_{-+}(s)\,\mathrm{d}s$$

$$P_+(r) = 1 - \int_0^r G_{+-}(s)\,\mathrm{d}s\,. \qquad (B3)$$

Therefore, the entire formalism hinges around being able to determine $P_-(r)$ and $P_+(r)$, through the simultaneous solution of (*B2*) and (*B3*), under the following obvious boundary condition,

$$\rho_- G_{-+}(r) = \rho_+ G_{+-}(r) \qquad (B4)$$

since electroneutrality requires $g_{-+}(r) = g_{+-}(r)$. For the present case, considering (*B3*) and (*B4*), we obviously have $P_-(r) = P_+(r)$ and $\rho_+ = \rho_-$, and by solving the integral equation it follows that,

$$P_-(r) = \left(1 + 4\pi\rho_+ \int_0^r g_{-+}(s) s^2\,\mathrm{d}s\right)^{-1}. \qquad (B5)$$

Finally, from (*B2*)–(*B5*),

$$G_{+-} = \frac{4\pi\rho_+ g_{-+}(r) r^2}{\left(1 + 4\pi\rho_+ \int_0^r g_{-+}(s) s^2\,\mathrm{d}s\right)^2} \qquad (B6)$$

which satisfies the required normalization, i.e.,

$$\int_0^\infty G_{-+}(r)\,\mathrm{d}r = 1 - \left(1 + 4\pi\rho_+ \int_0^\infty g_{-+}(r) r^2\,\mathrm{d}r\right)^{-1} = 1\,. \qquad (B7)$$

According to the Poirier and DeLap formalism, similar expressions can be derived for asymmetric ion-pairs, as discussed in the original paper.

This research was sponsored by the Division of Chemical Sciences, Geosciences, and Biosciences, Office of Basic Energy Sciences under contract number DE-AC05-00OR22725 with Oak Ridge National Laboratory, managed and operated by UT-Battelle, LLC.

REFERENCES

1. Baaden M., Burgard M., Boehme C., Wipff G.: *Phys. Chem. Chem. Phys.* **2001**, *3*, 1317.
2. Gloe K., Stephan H., Grotjahn M.: *Chem. Eng. Technol.* **2003**, *26*, 1107.
3. Moyer B. A., Bonnesen P. V. in: *Supramolecular Chemistry of Anions* (A. Bianchi, K. Bowman-James and E. Garcia-Espana, Eds). Wiley–VCH, New York 1997.
4. Hofmeister F.: *Arch. Exp. Pathol. Pharmacol.* **1888**, *24*, 247.
5. Kunz W., Lo Nostro P., Ninham B. W.: *Curr. Opin. Colloid Interface Sci.* **2004**, *9*, 1.
6. Sisson A. L., Clare J. P., Davis A. P.: *Chem. Commun.* **2005**, 5263.
7. Sisson A. L., Clare J. P., Taylor L. H., Charmant J. P. H., Davis A. P.: *Chem. Commun.* **2003**, 2246.
8. Levitskaia T. G., Marquez M., Sessler J. L., Shriver J. A., Vercouter T., Moyer B. A.: *Chem. Commun.* **2003**, 2248.
9. Chialvo A. A.: *Fluid Phase Equilib.* **1993**, *83*, 23.
10. Chialvo A. A., Cummings P. T., Simonson J. M., Mesmer R. E.: *J. Chem. Phys.* **1999**, *110*, 1075.
11. Bockris J. O. M., Reddy A. K. N.: *Modern Electrochemistry*, Vol. 1. Plenum Press, New York 1998.
12. Herdman G. J., Neilson G. W.: *J. Mol. Liq.* **1990**, *46*, 165.
13. Ohtaki H., Radnai T.: *Chem. Rev.* **1993**, *93*, 1157.
14. Hinton J. F., Amis E. S.: *Chem. Rev.* **1967**, *67*, 367.
15. Chialvo A. A., Kusalik P. G., Cummings P. T., Simonson J. M.: *J. Phys. Condens. Matter* **2000**, *12*, 3585.
16. Soper A. K.: *Faraday Discuss. Chem. Soc.* **1996**, *103*, 41.
17. Cartailler T., Kunz W., Turq P., Bellisent-Funel M.-C.: *J. Phys. Condens. Matter* **1991**, *3*, 9511.
18. Kunz W., Barthel J., Klein L., Cartaillert T., Turq P., Reindl B.: *J. Solution Chem.* **1991**, *20*, 875.
19. Chialvo A. A., Simonson J. M.: *J. Chem. Phys.* **2003**, *119*, 8052.
20. Chialvo A. A., Simonson J. M.: *J. Chem. Phys.* **2006**, 124.
21. Chialvo A. A., Simonson J. M.: *Mol. Phys.* **2002**, *100*, 2307.
22. Enderby J. E.: *Chem. Soc. Rev.* **1995**, *24*, 159.
23. Squires G. L.: *Introduction to the Theory of Thermal Neutron Scattering*. Dover Publications, Mineola 1996.
24. Soper A. K., Neilson G. W., Enderby J. E.: *J. Phys. C* **1977**, *10*, 1793.
25. Poirier J. C., DeLap J. H.: *J. Chem. Phys.* **1961**, *35*, 213.
26. Berendsen H. J. C., Grigera J. R., Straatsma T. P.: *J. Phys. Chem.* **1987**, *91*, 6269.
27. Dang L. X.: *J. Chem. Phys.* **1992**, *96*, 6970.

28. Wallen S. L., Palmer B. J., Fulton J. L.: *J. Chem. Phys.* **1998**, *108*, 4039.
29. van Veggel F., Reinhoudt D. N.: *Chem. Eur. J.* **1999**, *5*, 90.
30. Cannon W. R., Pettitt B. M., McCammon J. A.: *J. Phys. Chem.* **1994**, *98*, 6225.
31. Nose S.: *J. Phys. Soc. Jpn.* **2001**, *70*, 75.
32. Sears V. F.: *Neutron News* **1992**, *3*, 26.